Coating induced residual stress in nonoriented electrical steel laminations

Yaoyao Ding, Matthew Gallaugher, Nicolas Brodusch, Raynald Gauvin, and Richard R. Chromik[a)]
McGill University, Department of Mining and Material Engineering, Montreal, Quebec H3A 0C5, Canada

(Received 16 April 2014; accepted 5 August 2014)

To produce the magnetic core of electric motors, nonoriented electrical steels (NOESs) are used with an electrically insulating coating applied to the surface. Residual stress is induced during the coating process, which will alter the hardness and magnetic domain structure of the NOES. In this study, the effect of the coating is examined, specifically, its role in creating a residual stress near the coating/steel interface. This stress was investigated by the nanoindentation technique. With this method, a ~30 μm deep affected area was observed for NOES along both the rolling and transverse cross section directions, when in the presence of the coating. A biaxial tensile stress of ~200 MPa was calculated from the measured hardness values in the NOES, which was linked to variations in the magnetic domain structure near the interface. The observed magnetic domain structure was simplified by the reduction of supplemental domain structure near the coating/steel interface.

I. INTRODUCTION

Nonoriented Si–Fe steel is the key material for carrying magnetic flux in electric motors.[1] To produce a high efficiency electric motor, magnetic properties of the NOES have been widely studied, and found to be closely related to the steel chemistry, microstructure, and texture.[2–4] For further improving the motor efficiency, the importance of determining the residual stress field induced by manufacturing processes, such as stamping, welding, and coating processes, has been recognized.[5–7]

Electrical steels are typically used as thin laminations, each with an insulating coating, for better magnetic properties, environmental resistance, heat resistance, and lower core loss in the final product.[8] The insulating coating, applied to isolate each lamination electrically and reduce eddy current losses, is commonly made from a mixture of organic and inorganic compounds.[8] The application of the coating induces a nonuniform stress state in both the coating and the steel substrate.[9] The residual stress can be a result of not only temperature and humidity variations,[10] but also a misfit strain at the coating/steel interface.[11]

Stress in electrical steels is typically determined by the following methods: x-ray diffraction (XRD), magnetic Barkhausen noise, strip bending theory, and indentation. A few studies on the residual stress of the coating and the steel substrate have been carried out in the past.[12,13] More specifically for electrical steels, the stress induced by the coating process was mostly studied in grain oriented electrical steel (GOES) laminates.[6,14,15] Within the steel substrate, an average uniaxial tensile stress, ranging from 20 to 150 MPa, was estimated from strip bending theory.[6] The presence of the tensile stress was found to be associated with improved core loss of the coated GOES.[6] A similar beneficial effect from the presence of residual stress induced by coating was observed in NOES.[5] A directional core loss improvement was found, which was suggested to be related to a biaxial stress state.[5] Unfortunately, no quantitative measurements were carried out in this study about the stress magnitude. The studies on the effect of residual stress on core loss and stress estimation from strip bending theory only provide general understanding of the stress state at macroscale level. There is still a stress field at the microscale level that has not yet been explored well, especially in NOES. Nanoindentation has been applied to stress measurement due to surface modification[16] and thermal spray coating process[9] in stainless steel. Different from stress measurement by XRD, where accuracy is influenced by instrument setup, material grain size, and strain gradient of the target field,[17,18] nanoindentation has been successfully applied to obtain microstress information, including the stress affected zone and localized stress magnitude, with a lateral resolution as fine as 20 μm.

Nanoindentation has been developed and widely used in materials science for determining mechanical properties at the microscale level.[19–21] Hardness (H) and reduced modulus (E_r) values for a sample can be determined using the Oliver and Pharr (O&P) method.[19] Hardness has been shown to change as a function of the residual stress level, whereby it is increased by compression and

[a)]Address all correspondence to this author.
e-mail: richard.chromik@mcgill.ca
DOI: 10.1557/jmr.2014.218

 © Materials Research Society 2014

https://doi.org/10.1557/jmr.2014.218 Published online by Cambridge University Press

reduced by tension.[22] This relationship was first observed in nanoindentation experiments[23] and later verified by a numerical study[24] on aluminum alloys. To calculate the stress level, one of the three main approaches[22,25–27] developed is Suresh and Giannakopoulos (SG) method.[22] From the literature, it has been successfully applied to the stress measurements of plasma-spray coated stainless steel[9] and evaluation of an equibiaxial stress in thin carbon film.[28] To estimate the stress value using this approach, either previous material properties or presence of a reference are required to be known.

Another approach of confirming the presence of residual stress is through variations in magnetic domain structure. This magnetic domain structure change as a result of the stress introduced by the coating has been characterized mainly in GOES,[14,15,29] and only limited number of studies are available on NOES.[30] From these studies, a common feature was observed. The application of tensile stress resulted in a redistribution and increase in the number of 180° domain walls along the stress direction. If present, supplementary domain structures (the small domain features oriented in a different direction to the primary magnetization) were also decreased or eliminated under tension. This variation in magnetic domain structure can be directly observed using a scanning electron microscope (SEM).[31,32]

In this study, two types of commercial NOES were studied, and the residual stress induced by the coating process was investigated along different cross sections using both nanoindentation and SEM. The nature and magnitude of the stress were first calculated based on the hardness changes according to the SG method. Additionally, the presence of stress was then further confirmed by domain structure variations from direct magnetic domain imaging.

II. MATERIALS AND METHODS

A. Sample preparation

Two types of commercially available low carbon, 2.8% Si nonoriented electrical steels with a thickness of ~300 μm were investigated, in the fully-processed, i.e., stress relief annealed (SRA), and semi-processed (non-SRA) conditions. Small pieces (10 × 6 mm) were cut from long NOES strips using a slow speed diamond blade. The as-received strips were mounted in a rigid wax before cutting to provide mechanical support. After cutting, the small samples went through one of the three following procedures.

Procedure 1: NOES with coating intact

The samples were kept at the as-received state after cutting.

Procedure 2: NOES with coating removed

After cutting, coating from some non-SRA samples was carefully removed by 1 μm diamond suspension until it just disappeared. The progress of coating removal was monitored by color variation, from brown (coating) to brown/silver (steel). Hence, a minimum amount of the steel layer was removed.

Procedure 3: Vacuum-annealed NOES without coating

Coating was completely removed from pieces of non-SRA samples by mechanical grinding on 600 grit papers. The non-SRA samples without coating were then laboratory annealed in vacuum at 800 °C for 24 h followed by 10 h of slow cooling in a furnace.

All types of specimens with and without coating were mounted in epoxy resin at room temperature with conductive fillers added, as shown schematically in Fig. 1. The cross sections along the rolling direction (RD) and the transverse direction (TD) were investigated in this work. The mounted specimens were then mechanically ground on 600 grit papers for 20 min to remove the damaged layer due to cutting. The exposed cross sections of the strips were then further prepared by mechanically grinding up to 1200 grit papers and 24 h vibratory polishing with 0.05 μm colloidal silica. The same procedure was followed for preparing samples for both scanning electron microscopy and nanoindentation.

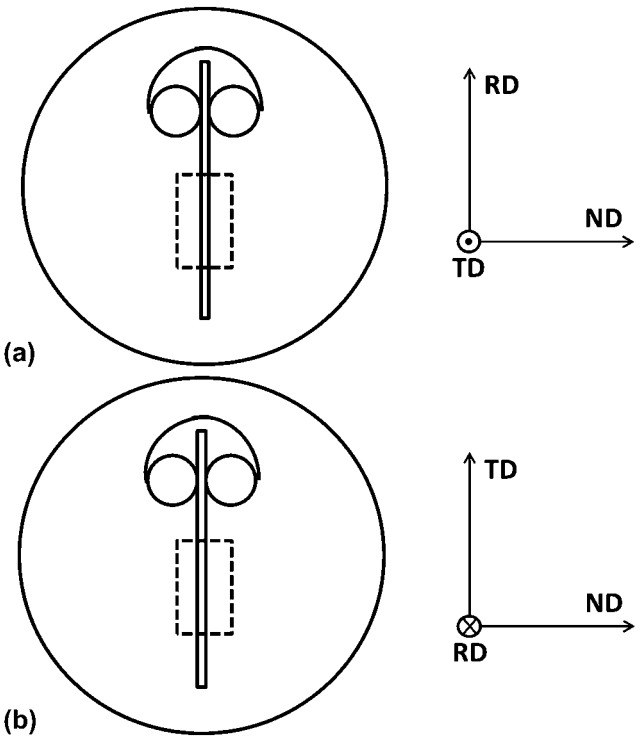


FIG. 1. Schematics of the mounted cross sections along (a) RD and (b) TD, where ND represents sample normal direction. The specimens were supported by plastic clips, and the areas enclosed by the dashed line were investigated.

https://doi.org/10.1557/jmr.2014.218 Published online by Cambridge University Press

B. Imaging and microanalysis by electron microscopy

A Hitachi SU-70 (Hitachi High-Technologies, Rexdale, ON, Canada) field-emission scanning electron microscope (FESEM) equipped with a Bruker Quantax 400 silicon drift detector (Bruker Canada, Milton, ON, Canada) as an energy dispersive spectrometer (EDS) was used to characterize the composition of the coating. The coating secondary electron (SE) and backscattered electron (BSE) micrographs were recorded at an accelerating voltage of 5 kV with a conventional Everhart-Thornley detector and a photodiode backscatter electron detector, respectively. X-ray microanalysis points were acquired at an accelerating voltage of 15 kV and the quantitative results were obtained using the standardless PhiRhoZ quantification mode from Bruker.

Grain orientations were determined by electron backscattered diffraction (EBSD) at 70° specimen tilt and an acceleration voltage of 20 kV with a Nordlys EBSD camera (Oxford Instruments, U.K.) with four forescatter detector (FSD) diodes. The collected signals were analyzed using HKL Channel 5 software. At the same sample position, magnetic domains were imaged using the bottom two FSD diodes at an acceleration voltage of 30 kV and a high probe current (~10 nA), as described elsewhere.[33] Both EBSD and magnetic domain imaging were carried out under the "field free" mode of the SEM.

C. Nanoindentation

Nanoindentation was carried out on the NOES specimens using a TriboIndenter (Hysitron, Minneapolis, MN), equipped with a three-sided pyramid Berkovich diamond tip. Before indenting on the NOES specimen, the tip area was calibrated by indenting on fused quartz. Indentations using a peak load of 5 mN (reaching a maximum penetration depth of ~200 nm) and a loading rate of 1 mN/s were performed in an array of lines of increasing distance from the coating. A 20 μm distance was kept among individual indents, and the lateral size for the residual indentation imprint was ~2 μm across. An example of the indentation sites is shown in a scanning electron microscopy micrograph in Fig. 2.

Both hardness (H) and reduced modulus (E_r) from each individual position were calculated using Eqs. (1) and (2), where P_{max} is the maximum loading force, A is the projected contact area, and S is the measured stiffness at the beginning of the unloading curve.[34] The projected contact area (A) can be calculated from the contact depth (h_c) according to the Oliver and Pharr method [Eq. (3)].[19]

$$H = \frac{P_{max}}{A} \quad , \tag{1}$$

$$E_r = \frac{S}{2}\frac{\sqrt{\pi}}{\sqrt{A}} \quad , \tag{2}$$

$$A = 24.5h_c^2 + C_1h_c^1 + C_2h_c^{1/2} \quad . \tag{3}$$

For quantitative stress measurement, the nature of the stress was first determined by the direction of the shift of the nanoindentation loading curve with regard to a reference loading curve (obtained from a stress free material), followed by the stress magnitude calculation using the following two equations.[22]

$$\frac{A_0'}{A'} = 1 - \frac{\sigma}{H_0}(\text{Tensile stress}) \quad , \tag{4}$$

$$\frac{A_0'}{A'} = 1 + \frac{\sigma \sin\alpha}{H_0}(\text{Compressive stress}) \quad . \tag{5}$$

where A' and A_0' are the projected contact areas from stressed and stress-free (reference) materials, respectively, H_0 is the hardness from the reference material, σ is the residual stress level, and α is the attack angle between the indenter and the material surface. Typical load–displacement curves obtained from the reference and stressed regions are shown in Fig. 3. For hardness and modulus data, all curves

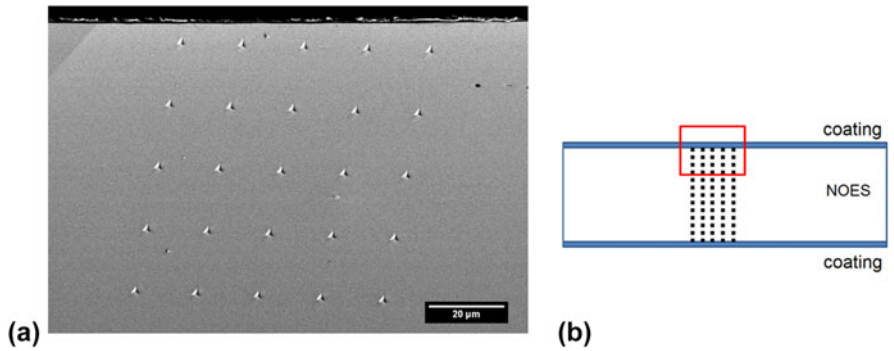


FIG. 2. Secondary electron micrograph of nanoindentation imprints (a) performed at a region indicated by the red square in a schematic diagram (b), where positions of indenting array are represented by black dots.

https://doi.org/10.1557/jmr.2014.218 Published online by Cambridge University Press

were included in the analysis. For an estimate of the stress by the SG method, analysis was conducted at the maximum penetration depth on the loading curves, where only curves with small pop-in loads similar to the curves shown in Fig. 3 were used. Some curves that exhibited higher pop-in loads (not shown) were not included in the SG analysis.

III. RESULTS AND DISCUSSION

A. NOES substrate characterization

The chemistry of both the non-SRA and SRA samples was obtained according to ASTM standards E1479 and E1019. Both samples were found to contain similar compositions (Table I). The sample grain size was measured according to the ASTM E112-10 standard using the Heyn lineal intercept procedure, where the number of intercepts from six drawn lines was counted. A measured average grain diameter of 186 μm for the non-SRA NOES was slightly larger than that of the SRA steel, which was 166 μm. Relative accuracies of 9% were obtained for both measurements (Table II).

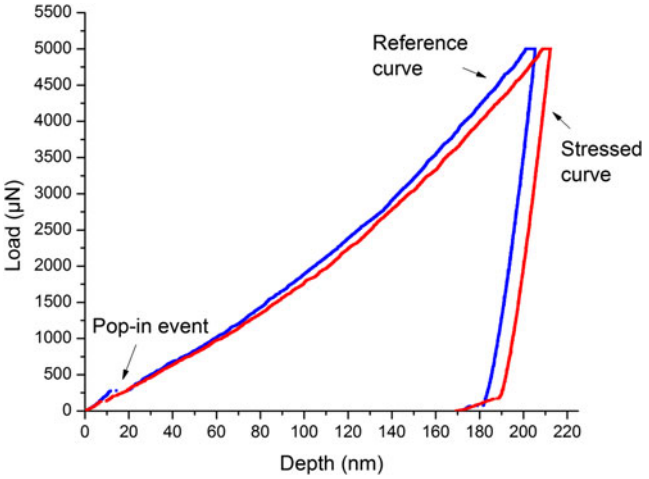


FIG. 3. Representative load–displacement curves obtained from reference and stressed regions of NOES by nanoindentation tests.

TABLE I. Chemical compositions of non-SRA and SRA samples (wt%).

NOES	C	O	Al	Si	Fe
Non-SRA	0.007	0.006	0.26	2.81	96.70
SRA	0.007	0.018	0.25	2.78	96.75

TABLE II. Grain size measurements of non-SRA and SRA samples.

NOES	ASTM grain size no.	Relative accuracy	Average mean lineal intercept (mm)	Average grain diameter (μm)
Non-SRA	2.6	9%	0.124	186
SRA	2.9	9%	0.111	166

B. NOES coating characterization

Based on the SE and BSE micrographs recorded in the SEM, the thickness of the coating was estimated to be around 1 μm and was uniformly distributed along the steel's surface. Within the thin coating, submicrometer pores of approximately 100 nm in diameter were observed, as shown in Fig. 4(a). Two spectra were obtained from the coating and the non-SRA NOES substrate, as shown in Fig. 4(b). The chemical compositions were determined by standardless x-ray microanalysis. The analysis indicated that the coating mainly consisted of C, O, Mg, Cr, and Fe, with traces of Si and Ca (Table III), which are commonly found in compositions of base/forsterite (Mg_2SiO_4) coating for grain oriented steel.[15]

C. Nanoindentation: Interior hardness

Hardness values were measured from the interior of the strip cross sections for non-SRA, SRA, and vacuum-annealed NOES samples. For each individual cross section, an average value was obtained from 6 indentations ~120 μm away from the coating/steel interface. As shown in Table IV, a similar hardness value was measured along both the RD and TD cross sections for all samples. No obvious anisotropic mechanical properties were detected. Comparing between non-SRA and SRA samples, the average hardness was reduced significantly after the stress relief annealing process, from 3.71 to 3.26 GPa. A similar magnitude of hardness reduction was produced with a 24 h laboratory annealing of the non-SRA sample without coating, where the average hardness was 3.24 GPa. The hardness from the vacuum-annealed specimen was treated as zero stress reference hardness for later residual stress calculations.

D. Nanoindentation: Near surface hardness profile

1. Coating intact versus removed

Prior to indenting on the non-SRA RD cross sections, the presence of the coating was confirmed by BSE micrographs. Then after nanoindentation, the distances between indents and the coating/steel interface (edge) were measured using SE micrographs. Line profiles of hardness and reduced modulus were calculated from ~5 individual large grains (≥100 μm in diameter) in contact with the coating. Based on channeling and optical contrast of the sample, crystal orientations were different at each probed grain. For a given distance from the coating/steel interface, an average hardness and modulus were calculated from ~40 measurements, where these data were taken from all the probed grains of differing orientations. This averaging was conducted as the general trend for all grains was similar and for this study we are focusing on the average overall effect of the coating. In future work, an examination of

https://doi.org/10.1557/jmr.2014.218 Published online by Cambridge University Press

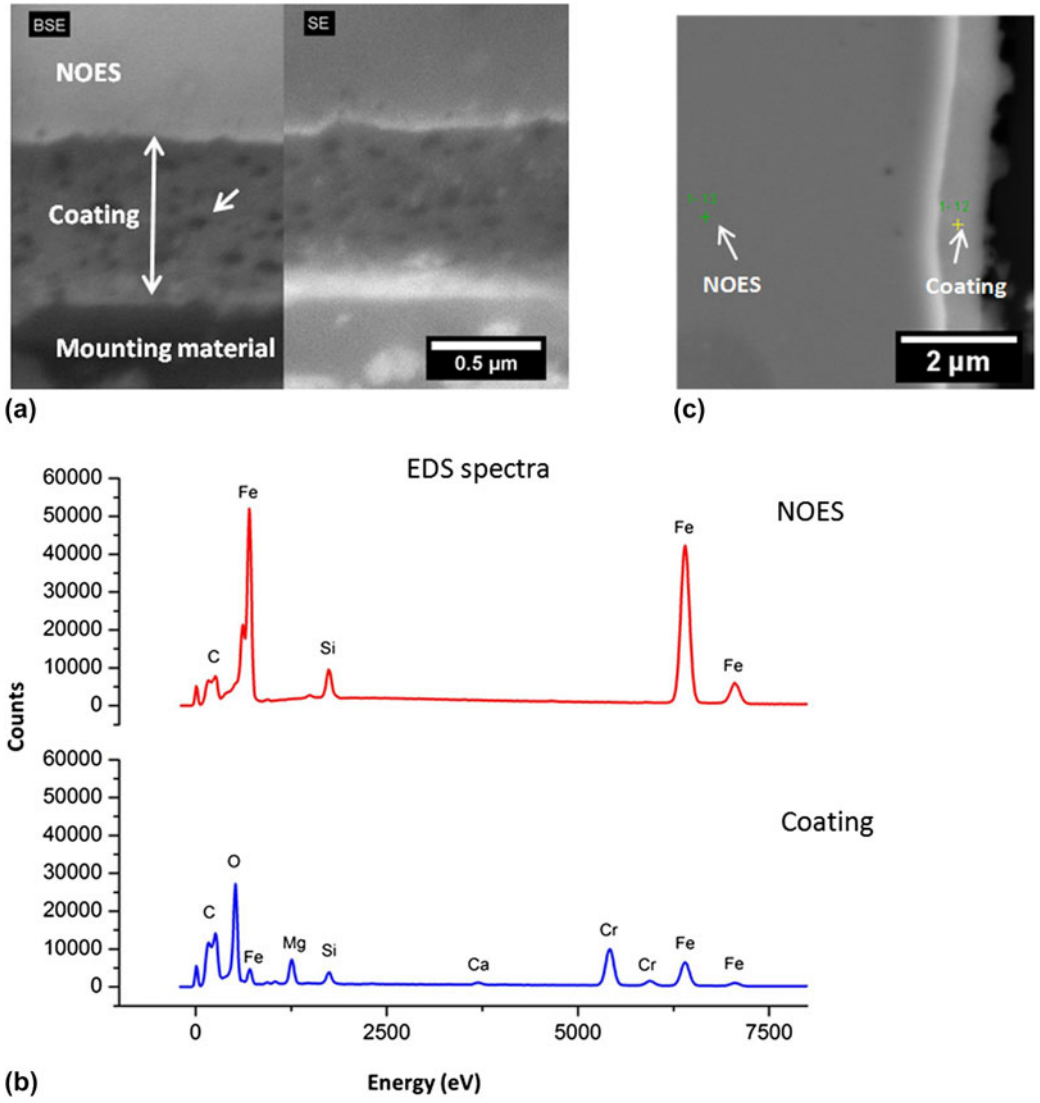


FIG. 4. BSE (left) and SE (right) micrographs of the coating are shown in (a). The coating thickness is approximately 1 μm and ~100 nm pores (indicated by the white arrow) are observed uniformly through the whole coating. Chemical composition measurements (in wt%) for both the non-SRA NOES and coating (b) were done by standardless point analysis using EDS. The positions, where the spectra were obtained, are indicated on the BSE image, as shown in (c).

TABLE III. Chemical composition (in wt%) for both the non-SRA NOES and coating by semiquantitative point analysis using EDS, where ND stands for not detected.

Spectrum	C	O	Al	Si	Fe	Mg	Ca	Cr
NOES	0.47	0.92	0.09	2.44	95.52	ND	ND	ND
Coating	12.58	24.98	0.01	0.59	31.66	5.06	0.21	20.63

the effect of crystallographic orientation on the stress profiles may be conducted.

The hardness variations with and without the presence of coating are shown in Fig. 5(a). With coating, the hardness was reduced to a minimum value of 3.0 GPa (at a distance of ~20 μm), followed by a hardness increase to a plateau of ~3.6 GPa as the distance was increased away from the coating/steel interface. Once the coating was removed, this hardness decrease was not observed, and a constant value of ~3.6 GPa was calculated through all distances from the interface that were tested. The absence of a hardness decrease upon coating removal implied that the hardness decrease in the coated NOESs was not created by the specimen mounting, but was a result of the presence of the coating.

For all indent distances to the edge tested, the average reduced modulus was calculated to be between 190 and 210 GPa for both samples (with and without the coating) as shown in Fig. 5(b). With the presence of the coating, a 10% reduction in modulus was observed at a distance of ~20 μm away from the coating/steel interface.

https://doi.org/10.1557/jmr.2014.218 Published online by Cambridge University Press

Possible reason is that the presence of residual stress alters material pile-up formation around the indents, which leads to errors in estimating the contact area for the modulus calculation. Similar effects have been reported in the literature.[23]

2. Variations of hardness along RD versus TD

Indentations were also carried out on RD and TD cross sections of the non-SRA and SRA samples following a similar procedure, both with intact coating. From both the non-SRA and SRA samples, similar trends of hardness variations were observed on both the RD and TD cross sections. As shown in Fig. 6, the trend of hardness variation remained indifferent of the cross section direction. A similar magnitude of hardness change was observed along both directions. However, once the hardness profile reached a plateau, a higher hardness value (3.5 GPa) was obtained from the non-SRA sample than that was obtained from the SRA sample (3.3 GPa). A similar magnitude of hardness (3.3 GPa) was observed in non-SRA, without coating, after laboratory vacuum annealing process [Fig. 6(c)]. From both the non-SRA and SRA samples, a region of lower hardness compared to the rest of the hardness versus position curve was observed at approximately 20 μm from the coating/steel interface.

TABLE IV. Hardness (H) and reduced modulus (E_r) values were determined by nanoindentation ~120 μm away from the coating/steel interface on both the RD and TD cross sections.

Sample	Coating	H_{RD} (GPa)	H_{TD} (GPa)	H_{ave} (GPa)	$E_{r,ave}$ (GPa)
Non-SRA	Yes	3.62 ± 0.16	3.75 ± 0.10	3.71 ± 0.13	204 ± 7
SRA	Yes	3.20 ± 0.10	3.32 ± 0.06	3.26 ± 0.10	200 ± 4
Vacuum annealed	No	3.29 ± 0.10	3.20 ± 0.10	3.24 ± 0.10	198 ± 5

3. Interpretation of hardness with regard to residual stress

The hardness from the plateau regions, where no significant effect of the coating was present, was compared firstly. Similar hardness values were obtained from both the SRA sample [Fig. 6(b)] and the non-SRA sample that had no coating and was laboratory annealed in vacuum [Fig. 6(c)]. However, a significant increase in hardness was observed in the non-SRA [Fig. 6(a)] from a similar region. The elevated amount of hardness could be explained by strain hardening effect due to NOES manufacture processes,[16,35] which was effectively removed by the annealing process.

With the hardness from the vacuum-annealed NOES sample serving as a nonstressed reference point, a lower hardness means the presence of tensile stress, and a higher hardness means the presence of compressive stress.[22] Since the hardness value in the plateau region from the SRA [Fig. 6(b)] sample was similar to that from the vacuum-annealed sample, the hardness changes observed from the region (i.e., close to the coating/steel interface) were mostly related to residual stress and not strain hardening. The dip in the near surface hardness profile indicated a tensile residual stress.

A similar hardness profile was obtained from the non-SRA [Fig. 6(a)] sample, where a dip followed by a plateau region was observed as the distance to the coating/steel interface increased. Compared to the vacuum-annealed sample, the elevated hardness in the interior is believed to be strain hardening related, as discussed before. Despite this, the level of hardness about 20 μm from the coating/steel interface is the same for both the non-SRA and SRA cases.

Based on the average hardness values obtained from multiple grains with varied crystal orientations, the stress values can be estimated using the SG method [Eqs. (4) and (5)].[22] This method assumes an equibiaxial stress

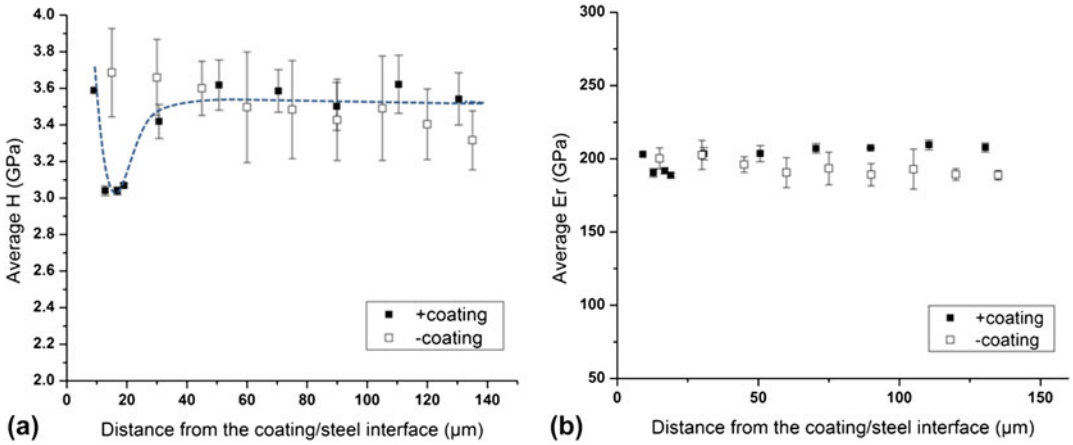


FIG. 5. Changes in average mechanical properties, (a) hardness (H) and (b) reduced modulus (E_r), along non-SRA rolling direction (RD) cross sections as the distance increased from the coating/steel interface. The dashed line shows the trend of hardness variation with coating.

https://doi.org/10.1557/jmr.2014.218 Published online by Cambridge University Press

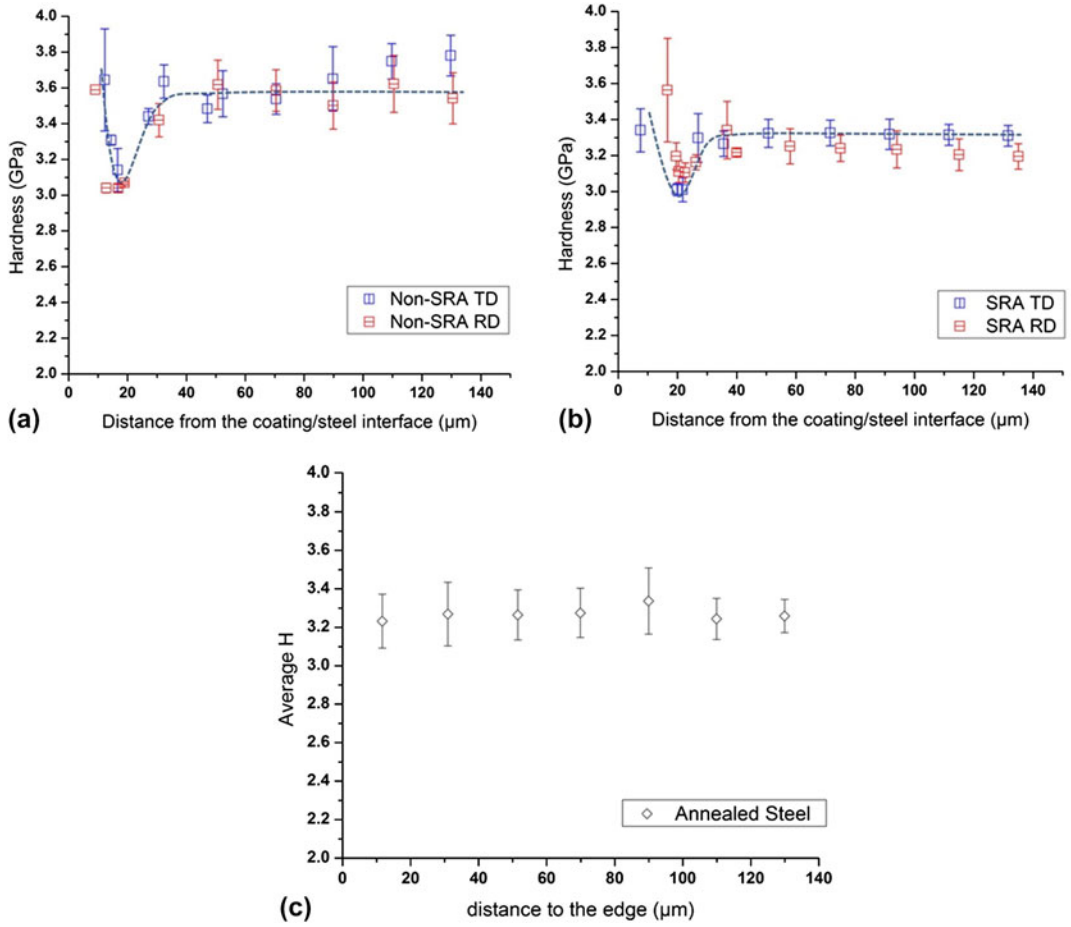


FIG. 6. Changes in hardness (H) along different cross section directions of non-SRA (a), SRA (b), and average from both directions of vacuum-annealed NOES (c) samples as the distance increased from the coating/steel interacting edge. The dashed line shows the trend of hardness variation.

state, which is not the case for our specimens. However, the SG method has been shown to provide reasonable prediction on an average residual stress value (average of the stresses along two axes).[36] Numerical simulations compared to nanoindentation showed that the average stress is a reasonable assumption.[37] We consider the utility of using the SG method here to that extent: to provide an estimate of the average stress imposed on the steel by the coating near the interface.

A nonstressed reference hardness (H_0) and projected contact area (A_0) were calculated by averaging the values obtained from the interior of the vacuum-annealed NOES. An average tensile stress of approximately 200 MPa was calculated for both the non-SRA and SRA samples. The magnitudes of the tensile stress from RD and TD were similar for both the non-SRA and SRA samples along both cross section directions. The average stress found here by nanoindentation is similar to reported values in the literature for a relatively thick TiN coating (>2 μm) on GOES, where the stress was measured by beam bending techniques.[6]

The residual stress induced by the coating process is primarily originated from a misfit strain between the coating and steel substrate,[11] but it can be affected by the changes in temperature and humidity.[10] As a result, a nonlinear stress gradient in the substrate is created, similar to the nonuniform stress field indicated by the hardness profiles shown in Figs. 5 and 6. The magnitude of the stress varied depending on the distance to the interface.[9,11] Despite the strain hardening effect, the presence of the tensile stress in the NOES improves its magnetic properties by reducing core loss along the direction of the stress field.[5] This improved core loss has been associated with better aligned and elongated magnetic domain structure as a result of the tensile stress,[14] and it can be tailored by optimizing the coating thickness.[5,6]

E. Variations in magnetic domain structure versus indentation profile

From the cross section of the coated non-SRA sample along the RD, grain crystallographic orientations were

https://doi.org/10.1557/jmr.2014.218 Published online by Cambridge University Press

determined by EBSD [Fig. 7(a)] and magnetic domain structure was observed [Fig. 7(b)] in the region close to the coating. Within the region shown in Fig. 7(a), β parameter (as defined for NOES in Ref. 33), was calculated, which is defined as the angle between the closest easy axis and the RD–TD plane, or surface of the sample. A larger value of β means a larger deviation between the easy axis and the surface. The grain indicated by a star had a relatively high β (9.6°), indicative of a finer, branched domain structure with supplementary domains.[33] This expected domain structure with supplementary domains was visible in the regions of the grain away from the coated surface, with the main domain alignment in the direction of the closest easy axis to the surface [black arrow in Fig. 7(b)]. However, in the region close to the coating/steel interface, the domain structure consisted of simple domains with no supplementary domain structure present. An average nanoindentation hardness profile was obtained by indenting in a 15 × 5 matrix (average of the 5 lines) with 20 μm apart within the same region as shown in Fig. 7(b). As shown in Fig. 7(c), hardness obtained from the region close to the coating/steel interface was lower than that obtained from the remaining area of the same grain. As discussed in the previous sections, this reduced hardness indicated the presence of tensile stresses.

The reduction in supplementary domain structure in the coating/steel interface region was consistent with the presence of tensile residual stress, which has been previously reported in GOES[14,15,29] and NOES.[30] With respect to the stress introduced by the coating, supplementary domain structure was significantly reduced or eliminated in NOES.[30] An equivalent of 5 MPa or less external tension was enough to achieve this modification on the domain structure.[15] The direct observation of reduction in supplementary domain structure with a SEM provides complementary information about the tensile residual stress zone near the coating/steel interface in addition to nanoindentation.

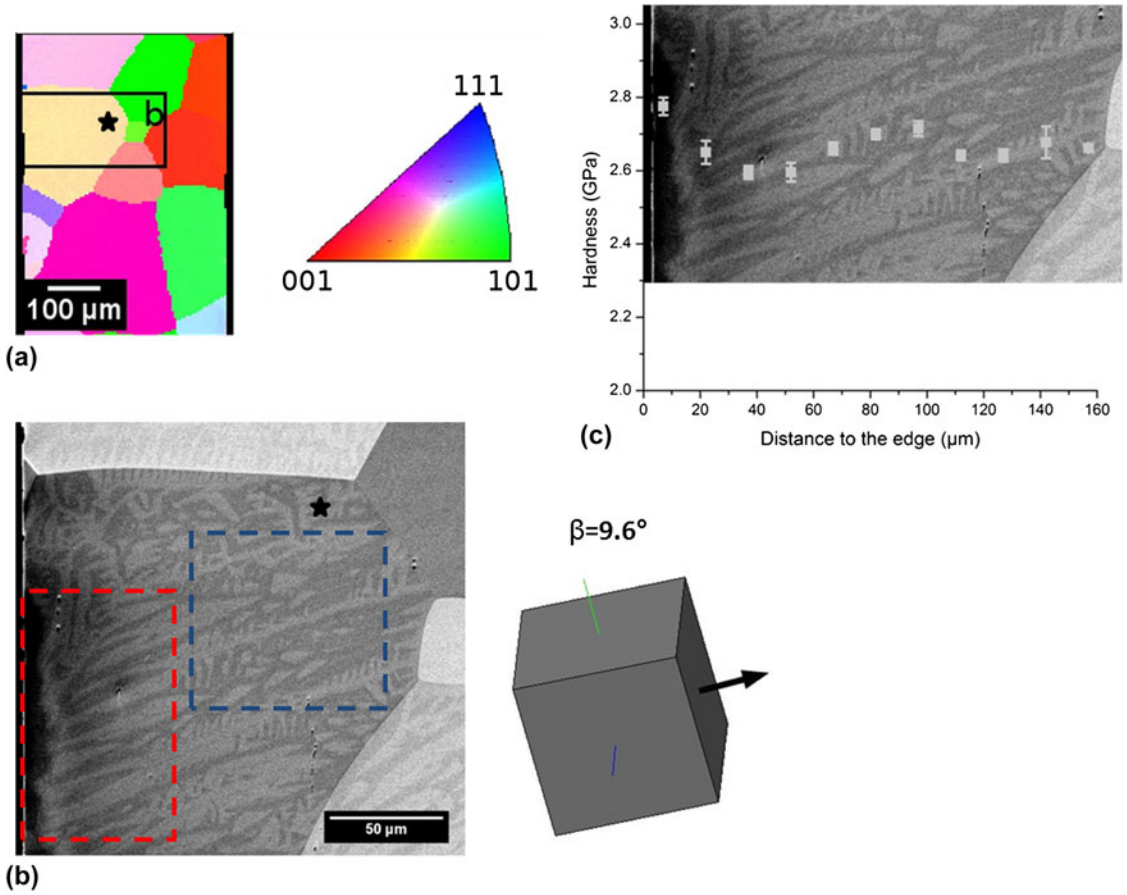


FIG. 7. Variation of magnetic domain structure as a result of stress. Crystal orientations were determined by electron backscatter diffraction (a) and illustrated by the crystal on the right (b) for the grain indicated by the star. The NOES texture parameter β for the same grain was calculated from the orientation.[33] Additionally, the stressed zone determined is outlined by the red dashed box on the left, and the unstressed zone is outlined by the blue dashed box on the right in (b). One nanoindentation hardness profile (c) was obtained from the same area as in (b).

https://doi.org/10.1557/jmr.2014.218 Published online by Cambridge University Press

IV. CONCLUSION

Nanoindentation was demonstrated to be a useful technique for probing the variation in mechanical properties in a NOES lamination. Hardness profiles as a function of position from the coating/steel interface allowed for a separation of various effects, such as strain hardening in non-SRA specimens and stress imposed by the coating for all specimens. Samples with coating removal were also used to demonstrate the differences in hardness profiles imposed by the coatings. In this study, the focus was on the average tensile stress effect the coating had on the stress state of the steel, which plays an important role in the magnetic properties in the intended application. An average tensile stress of 200 MPa was estimated for both the SRA and non-SRA samples, where this stress state was found approximately 20 μm from the coating/steel interface. The presence of the coating stress was further validated by the observation of magnetic domain structure combined to grain orientation using the forescatter detector of the EBSD system of a FESEM with a high accelerating voltage and probe current. The stressed magnetic domain structure in the stressed region was found to be simpler compared with that observed in the unstressed region within the single grain. This coating-induced tensile stress could potentially reduce the core loss and subsequently improve the efficiency of electric motors.

ACKNOWLEDGMENT

This research was supported by the Natural Science and Engineering Research Council (NSERC) and General Motors Canada. The authors would like to thank Dr. Florient Bridier and Dr. Philippe Bocher at École de technologie supérieure (ETS) for access to the SEM. Yaoyao Ding would like to thank Dr. Hendrix Demers for his help with reviewing this manuscript.

REFERENCES

1. Y. Oda, M. Kohno, and A. Honda: Recent development of non-oriented electrical steel sheet for automobile electrical devices. *J. Magn. Magn. Mater.* **320**, 2430 (2008).
2. L. Kestens, J.J. Jonas, P. Van Houtte, and E. Aernoudt: Orientation selection during static recrystallization of cross rolled non-oriented electrical steels. *Textures Microstruct.* **26–27**, 321 (1996).
3. K. Matsumura and B. Fukuda: Recent developments of non-oriented electrical steel sheets. *IEEE Trans. Magn.* **20**, 1533 (1984).
4. H. Shimanaka, Y. Ito, K. Matsumura, and B. Fukuda: Recent development of non-oriented electrical steel sheets. *J. Magn. Magn. Mater.* **26**, 57 (1984).
5. P. Chivavibul, M. Enoki, S. Konda, Y. Inada, T. Tomizawa, and A. Toda: Reduction of core loss in non-oriented (NO) electrical steel by electroless-plated magnetic coating. *J. Magn. Magn. Mater.* **323**, 306 (2011).
6. E. Beyer, L. Lahn, C. Schepers, and T. Stucky: The influence of compressive stress applied by hard coatings on the power loss of grain oriented electrical steel sheet. *J. Magn. Magn. Mater.* **323**, 1985 (2011).
7. R. Rygal, A.J. Moses, N. Derebasi, J. Schneider, and A. Schoppa: Influence of cutting stress on magnetic field and flux density distribution in non-oriented electrical steels. *J. Magn. Magn. Mater.* **215–216**, 687 (2000).
8. M. Lindenmo, A. Coombs, and D. Snell: Advantages, properties and types of coatings on non-oriented electrical steels. *J. Magn. Magn. Mater.* **215–216**, 79 (2000).
9. J. Zhu, H. Xie, Z. Hu, P. Chen, and Q. Zhang: Cross-sectional residual stresses in thermal spray coatings measured by Moire interferometry and nanoindentation technique. *J. Therm. Spray Technol.* **21**, 810 (2012).
10. D.Y. Perera: On adhesion and stress in organic coatings. *Prog. Org. Coat.* **28**, 21 (1996).
11. X.C. Zhang, B.S. Xu, H.D. Wang, Y.X. Wu, and Y. Jiang: Underlying mechanisms of the stress generation in surface coatings. *Surf. Coat. Technol.* **201**, 6715 (2007).
12. X.C. Zhang, B.S. Xu, H.D. Wang, and Y.X. Wu: An analytical model for predicting thermal residual stresses in multilayer coating systems. *Thin Solid Films* **488**, 274 (2005).
13. Y.C. Tsui and T.W. Clyne: An analytical model for predicting residual stresses in progressively deposited coatings. Part 1: Planar geometry. *Thin Solid Films* **306**, 23 (1997).
14. B. Fukuda, K. Satoh, T. Ichida, Y. Itoh, and H. Shimanaka: Effects of surface coatings on domain structure in grain oriented 3% Si-Fe. *IEEE Trans. Magn.* **17**, 2878 (1981).
15. S.D. Washko and E.G. Choby: Evidence for the effectiveness of stress coatings in improving the magnetic properties of high permeability 3%Si-Fe. *IEEE Trans. Magn.* **15**, 1586 (1979).
16. E. Frutos, M. Multigner, and J.L. Gonzalez-Carrasco: Novel approaches to determining residual stresses by ultramicroindentation techniques: Application to sandblasted austenitic stainless steel. *Acta Mater.* **58**, 4191 (2010).
17. B.B. He: *Two-Dimensional X-Ray Diffraction* (John Wiley & Sons, Hoboken, USA, 2009), p. 265.
18. Q. Luo and A.H. Jones: High-precision determination of residual stress of polycrystalline coatings using optimised XRD-sin$^2\psi$ technique. *Surf. Coat. Technol.* **205**, 1403 (2010).
19. W.C. Oliver and G.M. Pharr: An improved technique for determining hardness and elastic modulus using load and displacement sensing indentation experiments. *J. Mater. Res.* **7**, 1564 (1992).
20. T.L. Li, Y.F. Gao, H. Bei, and E.P. George: Indentation Schmid factor and orientation dependence of nanoindentation pop-in behavior of NiAl single crystals. *J. Mech. Phys. Solids* **59**, 1147 (2011).
21. Y. Lee, J.Y. Kim, J.S. Lee, K.H. Kim, J.Y. Koo, and D. Kwon: Using the instrumented indentation technique for stress characterization of friction stir-welded API X80 steel. *Philos. Mag.* **86**, 5497 (2006).
22. S. Suresh and A.E. Giannakopoulos: A new method for estimating residual stresses by instrumented sharp indentation. *Acta Mater.* **46**, 5755 (1998).
23. T.Y. Tsui, W.C. Oliver, and G.M. Pharr: Influences of stress on the measurement of mechanical properties using nanoindentation: Part I. Experimental studies in an aluminum alloy. *J. Mater. Res.* **11**, 752 (1996).
24. A. Bolshakov, W.C. Oliver, and G.M. Pharr: Influence of stress on the measurement of mechanical properties using nanoindentation: Part II. Finite element simulations. *J. Mater. Res.* **11**, 760 (1996).
25. S. Carlsson and P.L. Larsson: On the determination of residual stress and strain fields by sharp indentation testing: Part II: Experimental investigation. *Acta Mater.* **49**, 2193 (2001).
26. S. Carlsson and P.L. Larsson: On the determination of residual stress and strain fields by sharp indentation testing: Part I: Theoretical and numerical analysis. *Acta Mater.* **49**, 2179 (2001).

https://doi.org/10.1557/jmr.2014.218 Published online by Cambridge University Press

27. J.G. Swadener, B. Taljat, and G.M. Pharr: Measurement of residual stress by load and depth sensing indentation with spherical indenters. *J. Mater. Res.* **16**, 2091 (2001).
28. C.A. Taylor, M.F. Wayne, and W.K.S. Chiu: Residual stress measurement in thin carbon films by Raman spectroscopy and nanoindentation. *Thin Solid Films* **429**, 190 (2003).
29. N. Chukwuchekwa, A.J. Moses, and P. Anderson: Study of the effects of surface coating on magnetic Barkhausen noise in grain-oriented electrical steel. *IEEE Trans. Magn.* **48**, 1393 (2012).
30. K. Senda, A. Fujita, A. Honda, N. Kuroki, and M. Yagi: Magnetic properties and domain structure of nonoriented electrical steel under stress. *Electr. Eng. Jpn.* **182**, 10 (2013).
31. A. Hubert and R. Schafer: *Magnetic Domains: The Analysis of Magnetic Microstructures* (Springer, Berlin, Germany, 1998), p. 61.
32. D.E. Newbury, D.C. Joy, P. Echlin, C.E. Fiori, and J.I. Goldstein: *Advanced Scanning Electron Microscopy and X-ray Microanalysis* (Kluwer Academic/Plenum Publishers, New York, USA, 1986), p. 147.
33. M. Gallaugher, R.R. Chromik, N. Brodusch, and R. Gauvin: Magnetic domain structure and crystallographic orientation of electrical steels revealed by a forescatter detector and electron backscatter diffraction. *Ultramicroscopy* **142**, 40 (2014).
34. A.C. Fischer-Cripps: *Nanoindentation*, 3rd ed. (Springer, New York, USA, 2011), p. 31.
35. L. Kestens and S. Jacobs: Texture control during the manufacturing of nonoriented electrical steels. *Texture, Stress Microstruct.* **2008**, 173083 (2008).
36. Y.H. Lee and D. Kwon: Estimation of biaxial surface stress by instrumented indentation with sharp indenters. *Acta Mater.* **52**, 1555 (2004).
37. P. Mann: *Evaluation of Surface Modifications Introduced by Shot Peening of Aluminum Alloy 2024-T351* (Master's Thesis, McGill University, Canada, 2014), p. 65.

https://doi.org/10.1557/jmr.2014.218 Published online by Cambridge University Press